Available online at www.sciencedirect.com
SCIENCE DIRECT®
Journal of Power Sources 144 (2005) 183–190
JOURNAL OF POWER SOURCES
www.elsevier.com/locate/jpowsour

Electrode performance of layered $LiNi_{0.5}Ti_{0.5}O_2$ prepared by ion exchange

Masayuki Tsuda [a,*], Hajime Arai [b], Masaya Takahashi [a], Hideaki Ohtsuka [a], Yoji Sakurai [a], Koji Sumitomo [c], Hiroyuki Kageshima [c]

[a] *NTT Microsystem Integration Laboratories, NTT Corporation, 3-1, Morinosato Wakamiya, Atsugi, Kanagawa 243-0198, Japan*
[b] *NTT Environmental and Energy Laboratories, NTT Corporation, 3-1, Morinosato Wakamiya, Atsugi, Kanagawa 243-0198, Japan*
[c] *NTT Basic Research Laboratories, NTT Corporation, 3-1, Morinosato Wakamiya, Atsugi, Kanagawa 243-0198, Japan*

Received 1 November 2004; accepted 7 December 2004
Available online 10 February 2005

Abstract

A layered Li–Ni–Ti oxide including divalent nickel and tetravalent titanium with a Ni^{2+}/Ti^{4+} ratio of almost 1 was obtained by the ion exchange of a layered Na–Ni–Ti oxide precursor. By using various nickel and titanium sources, we obtained samples with different specific surface areas. Sample with larger specific surface areas had larger first charge capacities. However, a large irreversible capacity and poor cyclability were observed for all the samples when measured at room temperature. However, when we set the ambient temperature at 55 °C, the cyclability improved. This suggests that the lithium diffusion rate strongly affects the electrode performance of layered Li–Ni–Ti oxide. We also employed a first-principles calculation of the $LiNi_{0.5}Ti_{0.5}O_2/Ni_{0.5}Ti_{0.5}O_2$ system to evaluate its structural and voltage characteristics.
© 2005 Elsevier B.V. All rights reserved.

Keywords: Lithium battery; Positive electrode material; Lithium nickel titanium oxide; Layer structure; Ion exchange

1. Introduction

$LiNi_{0.5}Mn_{0.5}O_2$ performs extremely well as a positive electrode material for rechargeable lithium batteries, providing over 30 cycles with a capacity of 200 mAh g^{-1} [1]. This compound has a layered structure with a space group of $R\bar{3}m$, and contains divalent nickel and tetravalent manganese [2]. Additional research has shown that the redox center is divalent nickel, which becomes tetravalent due to oxidation during charging, and is then reduced to divalent nickel again during discharging at a 4 V plateau [2–4]. In contrast, manganese remains tetravalent during cycles at the 4 V plateau, and the absence of trivalent manganese contributes to its structural stability. Moreover, $LiCo_{0.5}Mn_{0.5}O_2$ has been reported to have first charge and discharge capacities of 220 and 125 mAh g^{-1}, respectively, while the valences of cobalt and manganese are unknown [5].

The synthesis of new compounds with divalent and tetravalent transition metal ions would provide candidates for new positive electrode materials. On this basis, we focused on Li–Ni–Ti oxide containing divalent nickel and tetravalent titanium. $Li_xNi_{1-y}Ti_yO_2$ ($0.1 \leq y \leq 0.5$) synthesized by simple calcination has been reported and it maintains its layered structure in the $y \leq 0.3$ region [6]. Moreover, some of the nickel in this compound is divalent. However, as the y value is over 0.3, the structure changes to a cubic rock-salt phase. Chang et al. [6] have not reported the electrode performance of $Li_xNi_{1-y}Ti_yO_2$ ($0.3 < y \leq 0.5$) with a cubic rock-salt phase. A compound with a cubic rock-salt phase rarely works as an electrode material. However, Prabarahan et al. have reported the electrochemical activity of nanostructured Li_2NiTiO_4 ($LiNi_{0.5}Ti_{0.5}O_2$) with a cubic rock-salt structure, which they obtained at low temperature (<300 °C) by using

* Corresponding author. Tel.: +81 46 240 3758; fax: +81 46 270 3721.
E-mail address: m-tsuda@aecl.ntt.co.jp (M. Tsuda).

0378-7753/$ – see front matter © 2005 Elsevier B.V. All rights reserved.
doi:10.1016/j.jpowsour.2004.12.012

a soft chemistry method [7]. They assume that this electrochemical activity is related to particle size. Noguchi et al. have also reported that the rock-salt structure $LiNi_{0.5}Ti_{0.5}O_2$ is active as an electrode material at 50 °C [8].

In our previous work, we reported preliminary results for layered structure $LiNi_{0.5}Ti_{0.5}O_2$ [9]. Kang et al. have reported on a compound with a similar composition, namely layered $Li_{0.9}Ni_{0.45}Ti_{0.55}O_2$ prepared by ion exchange using layered $Na_{0.9}Ni_{0.45}Ti_{0.55}O_2$ [10]. They stated that they chose this composition to avoid impurity phase NiO. However, as it is known that the electrochemical performance of $LiNi_{0.5}Mn_{0.5}O_2$ is good when the Ni/Mn molar ratio is close to 1 [1,11], we think it is desirable to prepare layered Li–Ni–Ti oxide with a Ni/Ti ratio close to 1.

We have reported the synthesis of layered $LiNi_{0.5}Ti_{0.5}O_2$, which includes divalent nickel and tetravalent titanium, by ion exchange in molten salt using layered $NaNi_{0.5}Ti_{0.5}O_2$ as a precursor [9]. In this paper, we attempt to improve the electrode performance of this layered $LiNi_{0.5}Ti_{0.5}O_2$ sample with various material sources. We prepared the layered $NaNi_{0.5}Ti_{0.5}O_2$ precursors using various nickel and titanium sources, and then characterized the ion exchanged layered $LiNi_{0.5}Ti_{0.5}O_2$ samples and measured the electrode performance. We also employed a first-principles calculation of the $LiNi_{0.5}Ti_{0.5}O_2/Ni_{0.5}Ti_{0.5}O_2$ system to evaluate its structural and voltage characteristics.

2. Experimental

We used three kinds of nickel and titanium sources to obtain the layered Na–Ni–Ti oxide precursors. One was $Ni(OH)_2$ and TiO_2 (Kanto Chemical Co., Inc.), as used in our previous report [9]. Another was nano-sized NiO and TiO_2 (NanoTek®, C. I. Kasei Co., Ltd.), which provided us with a finer powder sample. The third was $NiTiO_3$ (Kojundo Chemical Laboratory Co., Ltd.), whose Ni/Ti ratio was originally 1. As a sodium source, we used Na_2CO_3 (Kanto Chemical Co., Inc.). We prepared the layered Na–Ni–Ti oxide as follows [12]. The sodium, nickel and titanium sources were mixed with a molar ratio of Na:Ni:Ti = 1.1:1:1. An excess of Na_2CO_3 was added to prevent any loss of the sodium component by volatilization. The mixture was calcined at 700 °C for 12 h, and then heated at 950 °C for 36 h in an argon atmosphere. In contrast to the previously reported ion exchange method in organic solvents [10], we used $LiNO_3$ as a molten salt for the ion exchange from sodium to lithium. The mixture of $LiNO_3$ and Na-type precursor was heated at 270 °C for 3 h in an argon atmosphere. The Li/Na ratio of the $LiNO_3$ to the precursor was 5. After the heat treatment, the reaction mixture was washed with distilled water and acetone, and then filtered and dried at 80 °C in air.

Hereafter, we denote the layered Na–Ni–Ti oxide precursor as 'precursor' and the sample after ion exchange as 'sample', and indicate the different sources by using 'A' for $Ni(OH)_2$ and TiO_2, 'B' for nano-sized NiO and TiO_2, and 'C' for $NiTiO_3$. For example, 'sample B' indicates the Li–Ni–Ti oxide after ion exchange, where precursor Na–Ni–Ti oxide was prepared by using nano-sized NiO and TiO_2.

The obtained precursors and samples were characterized by X-ray diffraction (XRD (Rigaku, RINT-2550/PC, Cu Kα)) and by determining their chemical composition (using inductively coupled plasma spectrometry (ICP spectrometry (Seiko Instruments, SPS-1700)) and iodometry). We performed a Rietveld refinement of the precursors and samples with the aid of the computer program RIETAN2000 [13]. The morphology of the samples was observed with a scanning electron microscope (SEM (JEOL, JSM-5410)), and their specific surface areas were measured by the BET method (Quantachrome, NOVA2200). We determined the nickel and titanium valences using X-ray absorption spectroscopy (XAS, especially X-ray absorption near-edge structure (XANES) spectral analysis (High Energy Accelerator Research Organization, Photon Factory, Beam line BL12C)).

A first-principles calculation was employed using an ultrasoft pseudopotential method as implemented in CASTEP (Accelrys Inc., Materials Studio) [14,15].

The electrochemical performance of the samples was measured using a coin cell with a metallic lithium negative electrode. The positive electrode mixture consisted of 70 wt.% of the sample, 25 wt.% of acetylene black as a conductive agent and 5 wt.% of polytetrafluoroethylene as a binder. The electrolyte was a 1 mol dm^{-3} $LiPF_6$ solution consisting of equal volumes of ethylene carbonate and dimethyl carbonate. We measured the electrode performance with a current density of 0.1 mA cm^{-2} at room temperature. To measure the quasi open circuit voltage (QOCV) profile, we applied an intermittent current of 0.1 mA cm^{-2} for 2 h followed by a 6 h rest period.

For ex situ XRD, the coin cell was disassembled after a certain number of cycles and the positive electrode pellet was removed. This pellet was placed in a sealed sample holder with a polyimide film window to avoid exposing it to the atmosphere during the measurement. All these operations were performed in a dry air atmosphere.

3. Results and discussion

3.1. Characterization

Fig. 1 shows the XRD patterns of the obtained precursors. The colors of these fine powders ranged from pale green to yellow green. For precursors A and C, these samples included a slight amount of NiO impurity (Figs. 1(a) and (c)), despite the kind of sources. In contrast, Fig. 1(b) shows that precursor B included a slight amount of metallic Ni impurity, because the fine NiO powder was easily reduced in an argon atmosphere. There was a small broad unknown peak at around 40° in the patterns obtained for precursors B and C (Fig. 1(b) and (c)), and this peak vanished after the ion exchange. We eliminated this peak from our analysis by means of the Reitveld

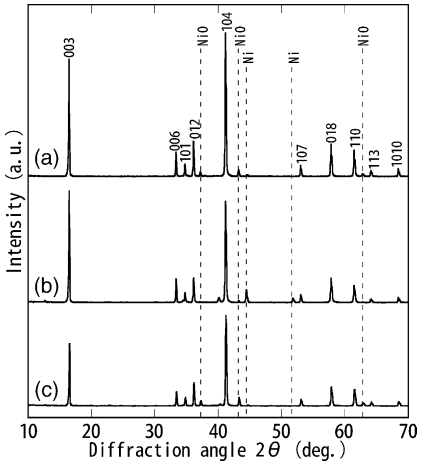

Fig. 1. XRD patterns of the obtained precursors: (a) precursor A, (b) precursor B and (c) precursor C.

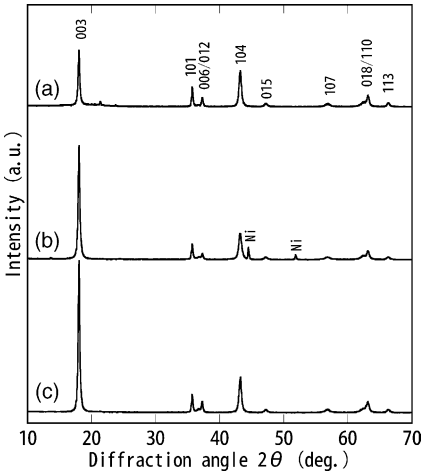

Fig. 2. XRD patterns of the obtained samples: (a) sample A, (b) sample B and (c) sample C.

refinement, etc. All the peaks, except for the slight impurity, were indexed in space group $R\bar{3}m$. With precursor B, the 003 peak intensity was as strong as the 104 peak. The nominal chemical compositions of the precursors are shown in Table 1. The Ni/Ti molar ratio of these precursors was almost 1. The presence of excess sodium and oxygen compared with the amount of transition metal was caused by excess Na_2CO_3.

Rietveld refinement was carried out for the space group $R\bar{3}m$ with Na in 3a (0,0,0) sites, with the same amount of Ni and Ti in 3b (0,0,0.5) sites and with O in 6c (0,0,z) sites. We assumed the impurities to be NiO (space group in Fm3m) for precursors A and C, and metallic Ni (space group in Fm3m) for precursor B. For precursor A, the Na–Ni–Ti oxide phase had lattice parameters of $a = 3.0099(2)$ and $c = 16.064(1)$ and the oxygen parameter $z = 0.2321(2)$ ($R_{wp} = 15.0$). The crystal lattice shrank compared with the published values (International Centre for Diffraction Data, Powder Diffraction File (ICDD PDF) #16-0251 $NaTiO_2$ ($a = 3.02$ and $c = 16.2$)). The calculated Na-O and (Ni, Ti)-O distances of 0.24 and 0.20 nm corresponded to the sum of the ionic radiuses of Na^+ (0.116 nm), Ni^{2+} (0.083 nm), Ti^{4+} (0.075 nm) and O^{2-} (0.126 nm) [16]. The refined lattice parameter of the impurity was $a = 4.1745(3)$ and corresponded to the NiO value ($a = 4.177$, ICDD PDF#44-1159). The Rietveld refinement also indicated that the mass ratio of NiO was 4%, suggesting that our precursor A consisted of 96% $Na_xNi_{0.48}Ti_{0.52}O_z$ and 4% NiO. We also analyzed precursors B and C in the same way. For precursor B, the lattice parameters of the Na–Ni–Ti oxide phase are $a = 3.0112(3)$, $c = 16.067(1)$ and $z = 0.2296(3)$ ($R_{wp} = 18.2$). The Rietveld refinement also indicated that precursor B consisted of 94% $Na_xNi_{0.49}Ti_{0.51}O_z$ and 6% Ni (not NiO). The Na–Ni–Ti oxide phase in precursor C had lattice parameters of $a = 3.0110(3)$ and $c = 16.069(1)$ and $z = 0.2337(2)$ ($R_{wp} = 16.4$), and precursor C consisted of 94% $Na_xNi_{0.48}Ti_{0.52}O_z$ and 6% NiO. The lattice parameters of the Na–Ni–Ti oxide phase were almost identical in all the precursors. We conclude that the Ni/Ti molar ratio of our precursors was closer to 1 than previously reported [10].

The fine powder samples were also pale green to yellow green after the ion exchange process, which indicates their low electronic conductivity. Table 1 shows the nominal chemical compositions of the samples. Although a small amount of sodium remained, it was largely exchanged for lithium. The ratios of the alkali ions, Li/(Ni, Ti) of about 0.8 and Na/(Ni, Ti) of about 0.1, were almost the same for each sample. The amounts of Ni and Ti were maintained during the ion exchange process. Fig. 2 shows the XRD patterns of the samples. These patterns were indexed in space group $R\bar{3}m$. Due to the strong orientation of these fine powdered samples, we were unable to obtain a satisfactory result with the Rietveld refinement. The lattice parameters were roughly $a = 2.95$ and $c = 14.8$ in space group $R\bar{3}m$. The lattice was stretched compared with that of $LiNiO_2$ ($a = 2.878$ and $c = 14.19$ (ICDD PDF#09-0063)).

The specific surface area of sample B was larger than those of samples A and C (Table 1). The grain size of the source

Table 1
Chemical compositions of precursors and samples

Precursor or sample	Nominal chemical composition	Mean valence of transition metals	Specific surface area ($m^2\ g^{-1}$)
Precursor A	$Na_{1.08}Ni_{0.49}Ti_{0.51}O_{2.07}$	3.06	–
Precursor B	$Na_{1.07}Ni_{0.50}Ti_{0.50}O_{2.06}$	3.05	–
Precursor C	$Na_{1.03}Ni_{0.49}Ti_{0.51}O_{2.02}$	3.01	–
Sample A	$Li_{0.80}Na_{0.12}Ni_{0.49}Ti_{0.51}O_{1.98}$	3.04	3.34
Sample B	$Li_{0.83}Na_{0.13}Ni_{0.49}Ti_{0.51}O_{1.99}$	3.02	5.34
Sample C	$Li_{0.81}Na_{0.11}Ni_{0.50}Ti_{0.50}O_{1.97}$	3.02	3.10

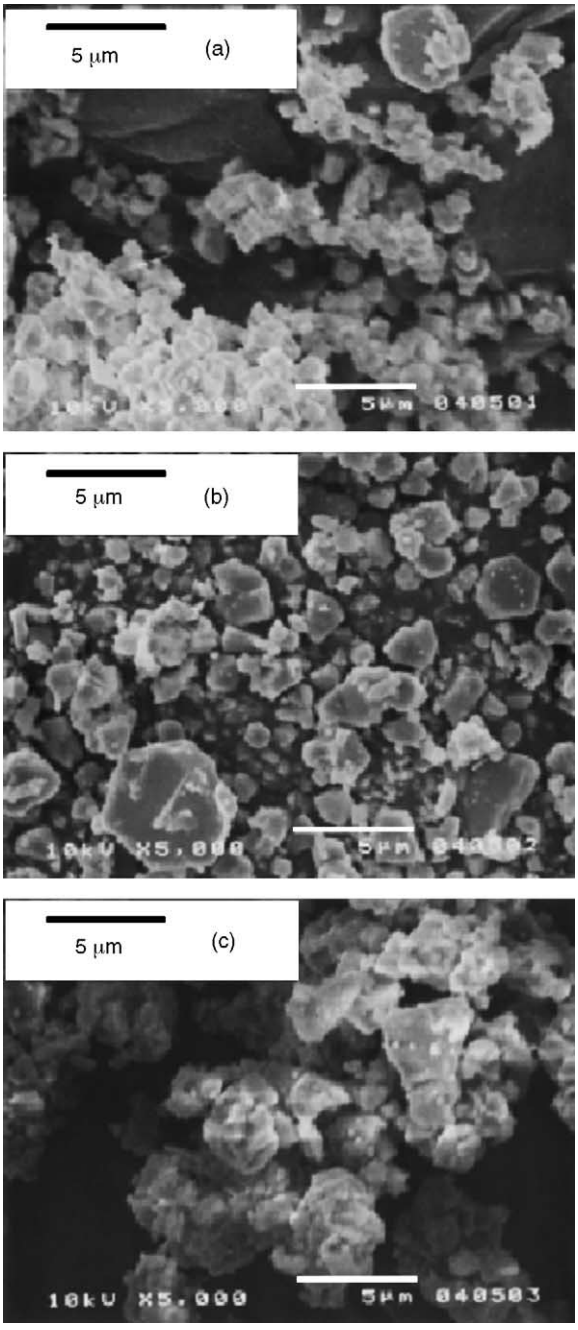

Fig. 3. SEM images of the obtained samples: (a) sample A, (b) sample B and (c) sample C.

material affected the specific surface area of the product material. SEM images (Fig. 3) of the samples also indicate that sample B was different from the other two samples. The particle size was 1–5 μm for all the samples. For samples A and C, the particles were agglomerated. In contrast, the sample B particles existed independently and no agglomeration was observed.

We determined the nickel and titanium valences by performing a XANES spectral analysis of precursor A and sample A. Fig. 4(a) and (b) show Ni and Ti K-edge XANES

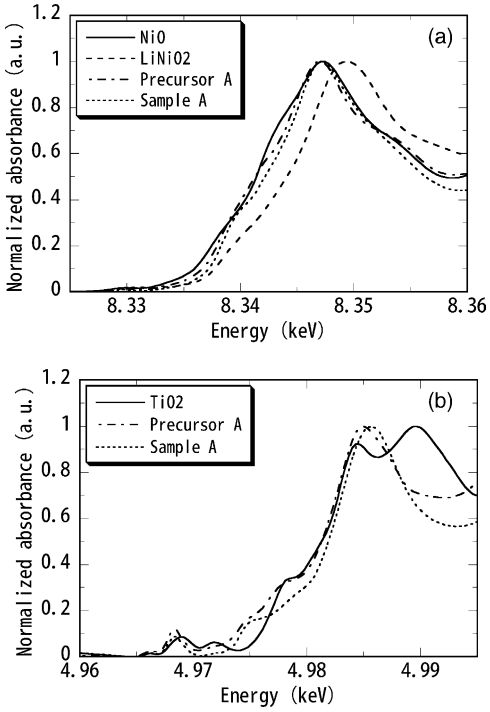

Fig. 4. (a) Ni K-edge and (b) Ti K-edge XANES spectra of precursor A and sample A.

spectra of precursor A and sample A, respectively. The Ni K-edge spectra of precursor A and sample A were similar to that of the Ni^{2+} reference, NiO. The peak energy was 8.347 keV and this value was smaller than the peak energy of $LiNiO_2$ (Ni^{3+} reference), 8.349 keV. The entire $LiNiO_2$ spectrum also shifted toward a higher energy than the other spectra. These observations suggest that the nickel in precursor A and sample A is in a divalent state. The Ti K-edge spectra of precursor A and sample A were similar to each other. Although the peak shape of the Ti^{4+} reference, rutile-type TiO_2, was different from those of precursor A and sample A, all the spectra had pre-edges at about 4.968 keV, and the maximum peak energies were also similar (about 4.985 keV). Moreover, there was no big shift among any of the spectra. Accordingly, we concluded that tetravalent titanium was present. The difference between the spectral shapes is probably caused by the different environment around the titanium ions. As shown in Table 1, the average valence of the transition metals, nickel and titanium, was approximately 3. This also suggests that precursor A and sample A consist of divalent nickel and tetravalent titanium with a Ni^{2+}/Ti^{4+} ratio of about 1.

A first-principles calculation for $LiNi_{0.5}Ti_{0.5}O_2$ has already been reported using a program called VASP [10]. Here, a complementary computational study was employed using an ultrasoft pseudopotential method as implemented in CASTEP [14,15]. The geometries and energies of $LiNi_{0.5}Ti_{0.5}O_2$ and $Ni_{0.5}Ti_{0.5}O_2$ were calculated in the generalized gradient approximation to density functional theory, with spin polarization. A supercell containing two units of

Table 2
Calculated and experimental structural parameters of $LiNi_{0.5}Ti_{0.5}O_2/Ni_{0.5}Ti_{0.5}O_2$ system

	a (Å)	b (Å)	c (Å)	β (degree)	Interlayer distance (Å)	Ni—O distance (Å)[a]	Ti—O distance (Å)[a]	Density ($g\,cc^{-1}$)
$LiNi_{0.5}Ti_{0.5}O_2$ (calc)	5.069	2.960	5.133	109.12	4.85	2.09	1.98	4.21
$LiNi_{0.5}Ti_{0.5}O_2$ (exp)	2.95	–	14.8	–	4.93	–	–	4.12
$Ni_{0.5}Ti_{0.5}O_2$ (calc)	5.063	2.935	5.597	107.70	5.33	1.92	1.98	3.58

[a] Multiply mean value.

$Li_xNi_{0.5}Ti_{0.5}O_2$ was described as monoclinic (P2/m), thus allowing nonequivalent distances for Ni–O and Ti–O bonds. Although the actual $LiNi_{0.5}Ti_{0.5}O_2$ material has a hexagonal unit cell, with our program no linear constraint was permitted that would allow us to calculate the hypothetic hexagonal cell.

The results are summarized in Table 2. The calculated lattice parameters of $LiNi_{0.5}Ti_{0.5}O_2$ were close to the experimental values. We found that the hypothetical compound $Ni_{0.5}Ti_{0.5}O_2$ had an interlayer distance that was 10% longer than that of the fully lithiated compound. We also confirmed that $LiNi_{0.5}Ti_{0.5}O_2$ and $Ni_{0.5}Ti_{0.5}O_2$ virtually have divalent and tetravalent nickel ions, respectively, while both have tetravalent titanium ions. This is in agreement with a previous report [10] and was expected from our XANES spectra. The Ni–O distance decreases greatly during the delithiation process, while the Ti–O distance remains unchanged. The calculated voltage was 3.3 V, using metallic lithium (body-centered cubic) as a negative electrode. We employed a similar calculation for $LiNi_{0.5}Mn_{0.5}O_2/Ni_{0.5}Mn_{0.5}O_2$, which gave us a voltage of 3.6 V. It is noteworthy that these computational methods often underestimate the voltage values [10]. Both the experiments and calculation have indicated that the $LiNi_{0.5}Mn_{0.5}O_2/Ni_{0.5}Mn_{0.5}O_2$ system exhibits a high voltage [1,17], and this suggests that the $LiNi_{0.5}Ti_{0.5}O_2/Ni_{0.5}Ti_{0.5}O_2$ system can also have a high voltage. At the same time we expect that the volumetric energy density of this system may not be very high, due to the low volumetric density of around 4.2, compared with $LiCoO_2$ (5.0) and $LiNiO_2$ (4.8).

3.2. Electrochemical performance

Fig. 5 shows the first to tenth charge–discharge curves of samples at voltages of 2.0–4.3 V. For all the samples, there was a large irreversible capacity within the first cycle, despite the low current density (0.1 mA cm^{-2}). For sample A, there was noticeable discharge capacity fading during the cycling. Sample B showed a large charge capacity and a severe irreversible capacity within the first cycle, but the cyclability was better than the others after the second cycle. Sample C had small capacities and poor cyclability. The samples with almost the same specific surface area (samples A and C) performed similarly despite the kind of nickel and titanium sources. In contrast, sample B, which had the largest specific surface area, had the largest first charge capacity and the best cyclability (after the second cycle), suggesting that the differ-

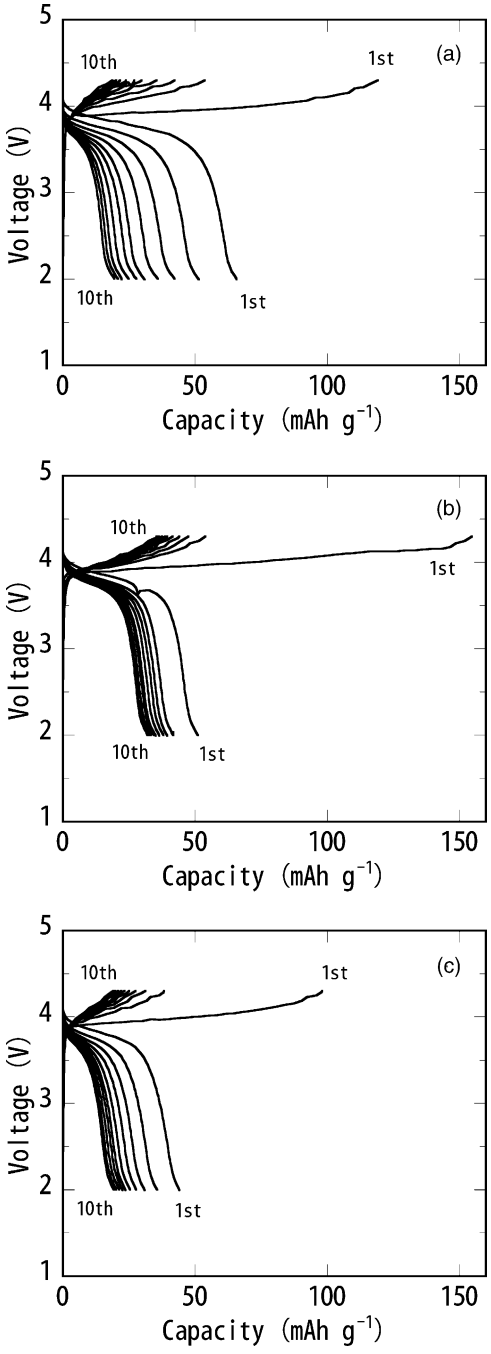

Fig. 5. Charge–discharge curves of samples at voltages of 2.0–4.3 V. The cycle number is indicated in the figures: (a) sample A, (b) sample B and (c) sample C.

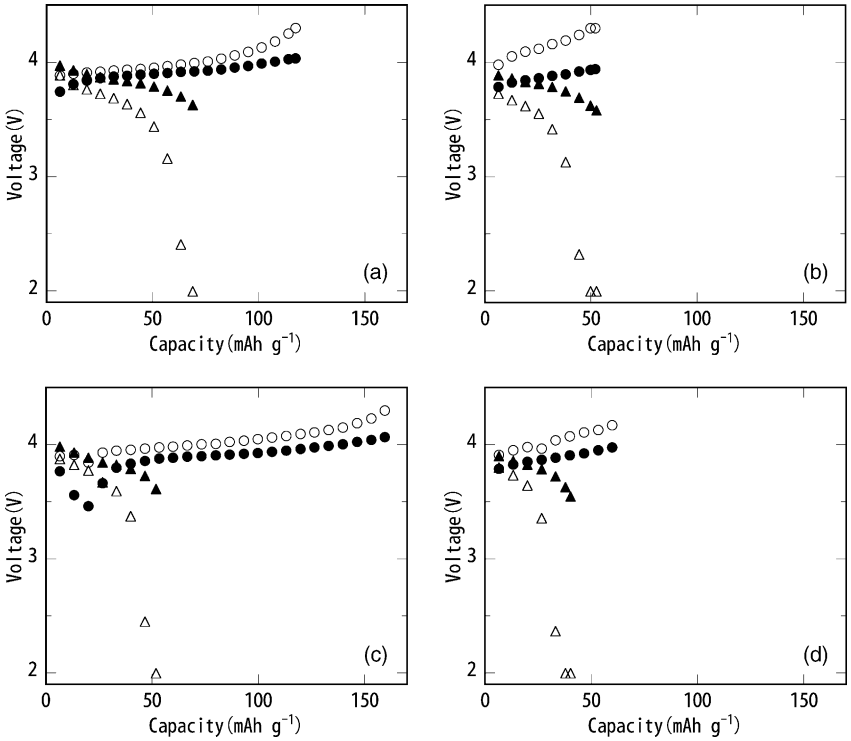

Fig. 6. QOCV profiles of samples A and B during the first and second charge–discharge processes; (a) sample A first cycle, (b) sample A second cycle, (c) sample B first cycle and (d) sample B second cycle. Filled symbols (●▲) and open symbols (○△) indicate QOCV and the voltage when current is flowing, respectively.

ence in specific surface area was clearly related to electrode performance.

This relationship was also observed in the overvoltage profiles. Fig. 6 shows the QOCV and current flow voltage profiles of samples A and B for the first and second charge/discharge processes at voltages of 2.0–4.3 V. For sample A, the overvoltage (the difference between the current flow voltage and QOCV) increased during the first charging process and became larger during the second charge process. The QOCV profile of sample C was similar to that of sample A. In contrast, the overvoltage was almost constant during the sample B charging process, and it was smaller than that of sample A during the second charging process. During the discharging process, the overvoltage increased greatly and a very large overvoltage was observed.

To discuss the cause of the inadequate electrode performance, we measured the electrode performance of sample A under various conditions. Fig. 7 shows the first to tenth charge–discharge curves of sample A, when we set the charge cut-off voltage at 5.0 V. The first charge capacity increased to 153 mAh g^{-1} but there was still severe irreversible behavior. The capacity increase caused by high-voltage charging was small. As the theoretical capacity of $LiNi_{0.5}Ti_{0.5}O_2$ is 290 mAh g^{-1}, the average Ni valence was close to three with the 5.0 V charging process. We suggest that it was difficult to oxidize the nickel to a tetravalent state under our experimental conditions. Fig. 8 shows ex situ XRD patterns of sample A after the first and tenth charge/discharge processes at voltages of 2.0–5.0 V. All the patterns were nearly same as that for pristine powder indexed in space group $R\bar{3}m$ (Fig. 2(a)). Although the 003, 101 and 110 peaks shifted and the 006 peak was more clearly observed in the discharged state than in the charged state, no dramatic phase transformation occurred during the cycling. Therefore, the inadequate electrode performance was not caused by phase transformation.

Kang et al. have reported that Ti^{4+} migration into the lithium layer, which is very difficult to observe by XRD analysis, may be the reason for the large irreversible capacity

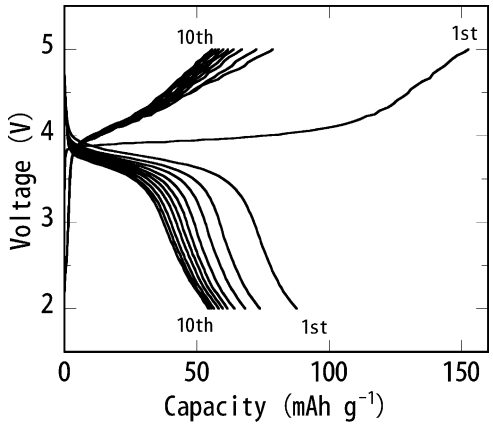

Fig. 7. Charge–discharge curves of sample A at voltages of 2.0–5.0 V. The cycle number is indicated in the figure.

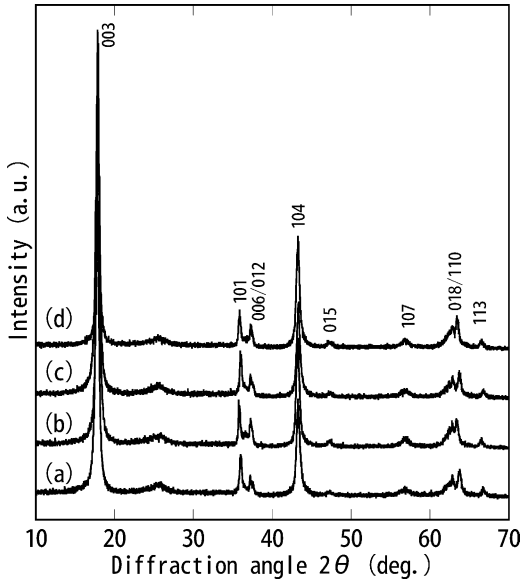

Fig. 8. Ex situ XRD patterns of sample A during cycling. The test cell was cycled at voltages of 2.0–5.0 V. The positive electrode pellets were removed after the (a) first charge, (b) first discharge, (c) tenth charge and (d) tenth discharge processes.

of the layered $Li_{0.9}Ni_{0.45}Ti_{0.55}O_2$ [10]. This could also apply to our layered $LiNi_{0.5}Ti_{0.5}O_2$ samples. Kang et al. have also reported that poor conductivity and large resistance lead to inadequate electrode performance. Moreover, we assume the low lithium diffusion rate to be another factor. As with $LiFePO_4$, whose performance was limited by the lithium diffusion rate, the particles with a larger specific surface area synthesized at a lower temperature showed better electrode performance [18]. Our samples performed similarly (Table 1 and Figs. 5 and 6).

If the low lithium diffusion rate limits the electrode performance, the measurement temperature may affect the electrode performance. So, we measured the electrode performance of sample A at 55 °C, and Fig. 9(a) shows the result. We set the cut-off voltage at 4.3 V to prevent the electrolyte decomposing at high temperature. Compared with the same sample measured at room temperature (Fig. 5(a)), the first charge capacity became small (about 100 mAh g^{-1}). However, the first discharge capacity of about 80 mAh g^{-1} was larger than that of all the samples measured at room temperature, and the irreversible capacity was greatly reduced. The cyclability was also improved, and the discharge capacity increased during cycling to reduce the irreversible capacity. The first charge capacity decreased as a result of the change in the measurement temperature. We believe that Ti^{4+} migration might occur during charging at high temperature and prevent lithium extraction. When we compare the charge/discharge curves at room and high temperatures (Figs. 5(a) and 9(a)), lithium extraction at over 100 mAh g^{-1} (in the $x > 0.35$ range, $Li_{0.80-x}Na_{0.12}Ni_{0.49}Ti_{0.51}O_{1.98}$) seemed to cause the irreversible capacity. In other words, there is a possibility that this material can be reversible in the $0 \leq x \leq 0.35$ range.

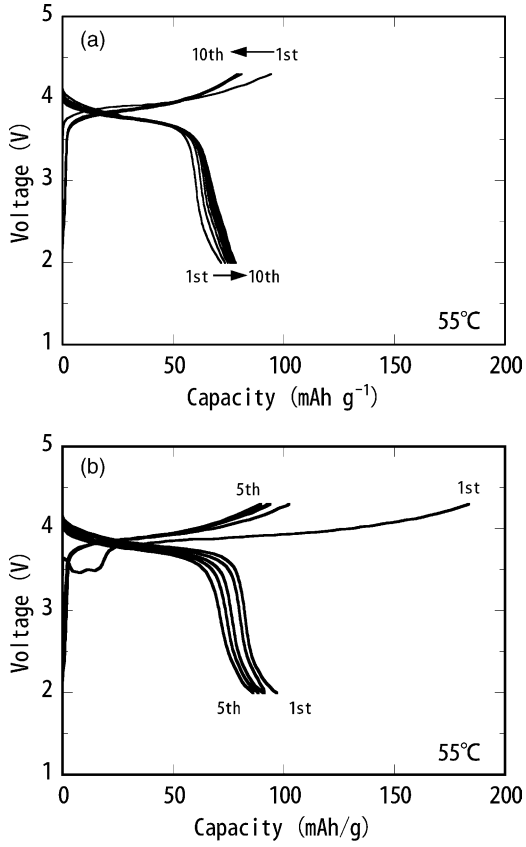

Fig. 9. Charge–discharge curves of (a) sample A and (b) sample B at 55 °C at voltages of 2.0–4.3 V. The cycle number is indicated in figures.

Therefore, we also carried out the measurement when we limit the charge capacity to 70 mAh g^{-1} ($x = 0.25$) at room temperature, but the irreversible capacity still remained. Therefore, we concluded that the great reduction in irreversible capacity and improved cyclability were affected by the measurement temperature. This suggests that the limited lithium diffusion rate is a factor that affects electrode performance.

We also measured the electrode performance of sample B at 55 °C. The sample with the largest specific surface area was expected to show the best performance at high temperature. The result is shown in Fig. 9(b). The first charge capacity of 184 mAh g^{-1} was the largest for all the samples in this study. There was a voltage drop during the first charging process. This behavior, which is also shown in Fig. 6(c), was certainly reproducible, and could be ascribed to the reaction of the metallic nickel contained in sample B. If we ignore the capacity during the voltage drop, the first discharge capacity was 160 mAh g^{-1} and there was none of the capacity reduction found with sample A (Fig. 9(a)), probably due to the large specific surface area of sample B. Unfortunately the irreversible capacity still remained, though sample B could perform cycles at about 90 mAh g^{-1}. When we compared the performance of samples A and B at 55 °C, we found that both were reversible at almost the same capacity of

80–90 mAh g^{-1} after the second cycle, despite the difference between their specific surface areas. These results indicate that the lithium diffusion rate strongly affects the electrode performance of layered $LiNi_{0.5}Ti_{0.5}O_2$.

4. Conclusion

The layered Li–Ni–Ti oxide containing divalent nickel and tetravalent titanium with a Ni^{2+}/Ti^{4+} ratio of almost 1 was obtained by the ion exchange of the layered Na–Ni–Ti oxide precursor. A First-principles calculation of this system suggests that it has a low volumetric density and a high voltage. The layered Li–Ni–Ti oxide with a specific surface area of about 3.0 $m^2\,g^{-1}$ (sample A) had first charge and discharge capacities of 120 and 65 mAh g^{-1}, respectively. When we set the cut-off voltage at 5.0 V for sample A, the first charge capacity increased to 150 mAh g^{-1}. The average nickel valence in the 5.0 V charged state was close to three, but we were unable to determine whether or not the nickel was oxidized into a tetravalent under our experimental conditions. For sample B, which had the larger specific surface area (5.0 $m^2\,g^{-1}$), we obtained the larger first charge capacity of 150 mAh g^{-1} and its cyclability after the second cycle was better than that of the other samples. When we measured the electrode performance of samples A and B at 55 °C, they showed better reversibility at capacities of 80–90 mAh g^{-1} after the second cycle, although their first charging behaviors were different due to their different specific surface areas. We therefore assume the low lithium diffusion rate to be another effective factor, in addition to the possible Ti^{4+} migration reported previously.

References

[1] Y. Makimura, T. Ohzuku, J. Power Sources 119–121 (2003) 156.
[2] W.-S. Yoon, C.P. Grey, M. Balasubramanian, X.-Q. Yang, J. McBreen, Chem. Mater. 15 (2003) 3161.
[3] H. Nakano, T. Nonaka, C. Okuda, Y. Ukyo, J. Ceram. Soc. Jpn. 111 (2003) 33.
[4] C.S. Johnson, J.-S. Kim, A.J. Kropf, A.J. Kahaian, J.T. Vaughey, L.M.L. Fransson, K. Edström, M.M. Thackeray, Chem. Mater. 15 (2003) 2313.
[5] A. Kajiyama, K. Takada, T. Inada, M. Kouguchi, S. Kondo, M. Watanabe, Solid State Ionics 149 (2002) 39.
[6] S.H. Chang, S.-G. Kang, S.-W. Song, J.-B. Yoon, J.-H. Choy, Solid State Ionics 86-88 (1996) 171.
[7] S.R.S. Prabaharan, M.S. Michael, H. Ikuta, Y. Uchimoto, M. Wakihara, IMLB 12 Meeting, Abs. 348 (2004).
[8] H. Noguchi, D. Li, T. Muta, IMLB 12 Meeting, Abs. 347 (2004).
[9] M. Tsuda, H. Arai, H. Ohtsuka, Y. Sakurai, Electrochem. Solid-State Lett. 7 (2004) A343.
[10] K. Kang, D. Carlier, J. Reed, E.M. Arroyo, G. Ceder, L. Croguennec, C. Delmas, Chem. Mater. 15 (2003) 4503.
[11] T. Ohzuku, Y. Makimura, Chem. Lett. (2001) 744.
[12] Y.-J. Shin, M.-Y. Yi, Solid State Ionics 132 (2000) 131.
[13] F. Izumi, T. Ikeda, Mater. Sci. Forum 321–324 (2000) 198.
[14] V. Milman, B. Winkler, J.A. White, C.J. Pickard, M.C. Payne, E.V. Akhmatskaya, R.H. Nobes, Int. J. Quant. Chem. 77 (2000) 895–910.
[15] M.S. Islam, R.A. Davies, J.D. Gale, Chem. Mater. 15 (2003) 4280.
[16] R.D. Shannon, Acta Cryst. A32 (1976) 751.
[17] J. Reed, G. Ceder, Electrochem. Solid-State Lett. 6 (2002) 145.
[18] M. Takahashi, S. Tobishima, K. Takei, Y. Sakurai, J. Power Sources 97–98 (2001) 508.